# The two types of ENSO in CMIP5 models

Seon Tae Kim[1] and Jin-Yi Yu[1]

[1]   In this study, we evaluate the intensity of the Central-Pacific (CP) and Eastern-Pacific (EP) types of El Niño-Southern Oscillation (ENSO) simulated in the pre-industrial, historical, and the Representative Concentration Pathways (RCP) 4.5 experiments of the Coupled Model Intercomparison Project Phase 5 (CMIP5). Compared to the CMIP3 models, the pre-industrial simulations of the CMIP5 models are found to (1) better simulate the observed spatial patterns of the two types of ENSO and (2) have a significantly smaller inter-model diversity in ENSO intensities. The decrease in the CMIP5 model discrepancies is particularly obvious in the simulation of the EP ENSO intensity, although it is still more difficult for the models to reproduce the observed EP ENSO intensity than the observed CP ENSO intensity. Ensemble means of the CMIP5 models indicate that the intensity of the CP ENSO increases steadily from the pre-industrial to the historical and the RCP4.5 simulations, but the intensity of the EP ENSO increases from the pre-industrial to the historical simulations and then decreases in the RCP4.5 projections. The CP-to-EP ENSO intensity ratio, as a result, is almost the same in the pre-industrial and historical simulations but increases in the RCP4.5 simulation. **Citation:** Kim, S. T., and J.-Y. Yu (2012), The two types of ENSO in CMIP5 models, *Geophys. Res. Lett.*, *39*, L11704, doi:10.1029/2012GL052006.

## 1.  Introduction

[2]  It has been increasingly recognized that two different flavors or types of El Niño-Southern Oscillation (ENSO) occur in the tropical Pacific [e.g., *Wang and Weisberg*, 2000; *Trenberth and Stepaniak*, 2001; *Yu and Kao*, 2007; *Ashok et al.*, 2007; *Kao and Yu*, 2009; *Kug et al.*, 2009]. The two types of ENSO are the Eastern-Pacific (EP) type that has sea surface temperature (SST) anomalies centered over the eastern tropical Pacific cold tongue region, and the Central-Pacific (CP) type that has the anomalies near the International Date Line [*Yu and Kao*, 2007; *Kao and Yu*, 2009]. In the literature, the non-conventional type of El Niño (i.e., the CP El Niño) has also been referred to as Date Line El Niño [*Larkin and Harrison*, 2005], El Niño Modoki [*Ashok et al.*, 2007], or Warm Pool El Niño [*Kug et al.*, 2009]. Several recent observational studies have indicated that the CP El Niño has been intensified in the past three decades [*Lee and McPhaden*, 2010] and that the climate impacts of the CP and EP types of ENSO can be distinctly different. For instance, the impact of the CP ENSO on winter surface air temperatures over the United States was found to be characterized by an east-west dipole pattern rather than the well-known north-south dipole pattern associated with the EP ENSO [*Mo*, 2010]. In the Atlantic, the CP El Niño tends to increase the frequency of Atlantic hurricanes, which is opposite to the impact produced by the EP El Niño [*Kim et al.*, 2009]. In the Southern Hemisphere, *Lee et al.* [2010] identified the large impacts of the 2009-10 CP El Niño on the warming in the South Pacific Ocean and west Antarctica and discussed the possible role of the increasing intensity of CP El Niño. *Ding et al.* [2011] also related the west Antarctica warming with the three-decade warming trend in the central equatorial Pacific, which was attributed to increasing intensity and frequency of CP El Niño by *Lee and McPhaden* [2010]. These findings point to a need to examine the different flavors or types of ENSO in the climate models used in the Intergovernmental Panel on Climate Change (IPCC) reports that aim to project future changes in climate variability modes (including ENSO) and their climate impacts.

[3]  The existence of the two types of ENSO has been considered in several studies that evaluated the performance of the coupled climate models from the Coupled Model Intercomparison Project Phase 3 (CMIP3) [*Meehl et al.*, 2007] in simulating ENSO [e.g., *Yu and Kim*, 2010; *Ham and Kug*, 2012]. *Yu and Kim* [2010], for example, documented the intensity, ratio, and leading frequency of the EP and CP ENSOs in the CMIP3 pre-industrial simulations and concluded that about nine of the nineteen models realistically simulate the intensity of the two types of the ENSO. Recently, the CMIP5, which include generally higher resolution models and a broader set of experiments relative to CMIP3, has been coordinated to be used in the IPCC Fifth Assessment Reports [*Taylor et al.*, 2012]. In this study, the two types of ENSO in the CMIP5 models are examined and compared with the CMIP3 models to gauge the improvement in performance from CMIP3 to CMIP5 models. A group of CMIP5 models that realistically simulate these two types of ENSO are then identified and used as the "best model ensemble" to examine changes in the two types of ENSO from the pre-industrial simulation to the historical simulation and the future climate projection. The results obtained in this study indicate that the EP and CP ENSO may not respond in the same way to climate change.

## 2.  Data and Method

[4]  In this study, the two types of ENSO simulated in the pre-industrial, historical, and future projection runs of CMIP5 models are analyzed. For the pre-industrial simulations, a total of twenty CMIP5 models are available for analysis. The names of these models are listed in the legend of Figure 2a. For the future climate projections, we choose to analyze the Representative Concentration Pathways 4.5 (RCP4.5) experiments because more models are available for

---

[1]Department of Earth System Science, University of California, Irvine, California, USA.

Corresponding author: J.-Y. Yu, Department of Earth System Science, University of California, Irvine, CA 92697-3100, USA. (jyyu@uci.edu)

analysis in this intermediate stabilization scenario. In this scenario, the target radiative forcing near year 2100 is set to be equal to 4.5 $Wm^{-2}$. Only thirteen of the twenty CMIP5 models provide SST outputs from their pre-industrial, historical, and RCP4.5 simulations. These thirteen models were used in the analysis of the response of the two types of ENSO to changes in atmospheric $CO_2$ concentrations. These models are indicated by an asterisk in the legend of Figure 2a. We analyzed the first 200 years of the pre-industrial simulations, roughly the years 1860–2005 of the historical simulations, and roughly the years 2006–2100 of the RCP4.5 projections. The exact lengths of the simulations vary slightly from model to model. The Extended Reconstruction of Historical Sea Surface Temperature version 3 (ERSST V3) data [*Smith and Reynolds*, 2003] are used to provide SST observations for the period 1950–2010. Monthly SST anomalies from the observations and the coupled models are calculated by removing the monthly mean climatology and the trend.

[5] To identify the two types of ENSO in the CMIP5 coupled models and the observations, we use a combined regression-Empirical Orthogonal Function (EOF) analysis [*Kao and Yu*, 2009; *Yu and Kim*, 2010]. We first remove the tropical Pacific SST anomalies that are regressed with the Niño1 + 2 (0°–10°S, 80°W–90°W) SST index and then apply EOF analysis to the remaining (residual) SST anomalies to obtain the SST anomaly pattern for the CP ENSO. Similarly, we subtract the SST anomalies regressed with the Niño4 (5°S–5°N, 160°E–150°W) index from the total SST anomalies and then apply EOF analysis to identify the leading structure of the EP ENSO. We remove not only the simultaneous regression but also the regression at lags −3, −2, −1, +1, +2, and +3 months using a linear multiple regression method to account for the possible propagation of SST anomalies.

## 3. Results

[6] Figure 1 shows the spatial patterns of the leading EOF modes for the EP and CP types of ENSO obtained by the regression-EOF method from the pre-industrial simulations of the twenty CMIP5 models. In the figure, the loading coefficients for the EOFs are scaled by the square root of their corresponding eigenvalues to represent the standard deviations (STD) of each of the EOF modes. Although discrepancies exist in the detailed realism of the simulated spatial patterns, several models are able to reproduce the observed features of the two types of ENSO, in which the EP type is characterized by SST variability extending from the South American Coast into the central Pacific along the equator and the CP type by SST variability centered in the central tropical Pacific (between 160°W and 120°W) that also extend into the subtropics of both hemispheres. We notice that the observed characteristic of the EP ENSO in which maximum SST variability is located immediately off the South American Coast is well captured by several CMIP5 models (e.g., GFDL-ESM2G, MIROC5, MPI-ESM-LR, MPI-ESM-P), whereas this feature was not as well captured in the CMIP3 models [see *Yu and Kim*, 2010, Figure 1]. The average pattern correlation coefficients between the simulated and observed EP and CP ENSOs for the CMIP5 models are 0.82 and 0.71, respectively. These values are larger than the CMIP3 pattern correlation coefficients (0.75 for the EP ENSO and 0.62 for the CP ENSO). Also, the inter-model

deviation of the pattern correlation coefficients is reduced from the CMIP3 to CMIP5 for the CP ENSO (from ±0.19 to ±0.13) but about the same for the EP ENSO (from ±0.17 to ±0.18).

[7] Using the scaled EOFs (Figure 1), we compute the maximum STDs between 10°S–10°N and 120°E–70°W to quantify the intensities of the two types of ENSO. Figure 2a displays a scatter diagram of the EP versus CP ENSO intensity from the CMIP5 simulations. The observed intensities calculated from the ERSST dataset (the gray point) are about 0.7°C for the CP ENSO and 1.0°C for the EP ENSO, indicating that the observed EP ENSO is stronger than the CP ENSO by about 40%. In order to determine which models produce realistically strong EP and CP ENSOs, we use the lower limit of the 95% significance interval of the observed ENSO intensities (using an F-test) as the criteria. The limits turn out to be 0.78°C for the EP ENSO and 0.51°C for the CP ENSO. Based on these criteria, nine of the twenty CMIP5 models (CNRM-CM5, GFDL-ESM-2G, GFDL-ESM2M, GISS-E2-H, HadGEM2-CC, HADGEM2-ES, MPI-ESM-LR, MPI-ESM-P, Nor-ESM1-M) simulate both the EP and CP ENSOs with realistically strong intensities. We also notice that it is more difficult for the models to produce realistically strong EP ENSOs than to produce strong CP ENSOs. Eleven (55%) of the twenty CMIP5 models fail to reach the lower intensity limit of the observed EP ENSO, while only 30% of the models fail to reach the limit of the CP ENSO.

[8] To compare the CMIP5 models' performance to that of the CMIP3 models, a similar scatter plot of the EP and CP ENSO intensities from *Yu and Kim* [2010] for the CMIP3 models is reproduced here in Figure 2b. We first notice that the percentage of models that can simulate both types of ENSO with realistically strong intensity (i.e., those models inside the blue squares in Figure 2) is similar in the CMIP5 models (45%; nine out of the twenty models) and CMIP3 models (47%; nine out of the nineteen models). In this regard, it can be concluded that there are no dramatic differences between these two generations of coupled climate models in the simulation of the two types of ENSO. However, some improvements in the simulations of the two types of ENSO can be identified in the CMIP5 models. Most importantly, the points produced from the CMIP5 models (Figure 2a) are less diverse than those from the CMIP3 models (Figure 2b). The CMIP3 models are more clearly separated into a group that produces strong ENSO intensities and a group that produces weak ENSO intensities. In CMIP5, the ENSO intensities simulated by the models converge into one single group closer to the observations. A closer inspection reveals that the reduction of the inter-model diversity in the simulated ENSO intensities is particularly significant for the EP type of ENSO. This is demonstrated in Figure 3, where the multi-model means of the ENSO intensities and their inter-model deviations (i.e., the STD) are shown for both the CMIP3 and CMIP5 models. The inter-model deviation (indicated by the colored vertical lines in Figure 3) is decreased in the CMIP5 compared to the CMIP3 models for both ENSO types. In particular, the reduction is much larger for the EP type than for the CP type. The inter-model STD of the EP ENSO intensities is 0.30°C among the CMIP3 models but only 0.18°C among the CMIP5 models, which is a statistically significant improvement at the 95% level according to an F-test. The reduction of the inter-model
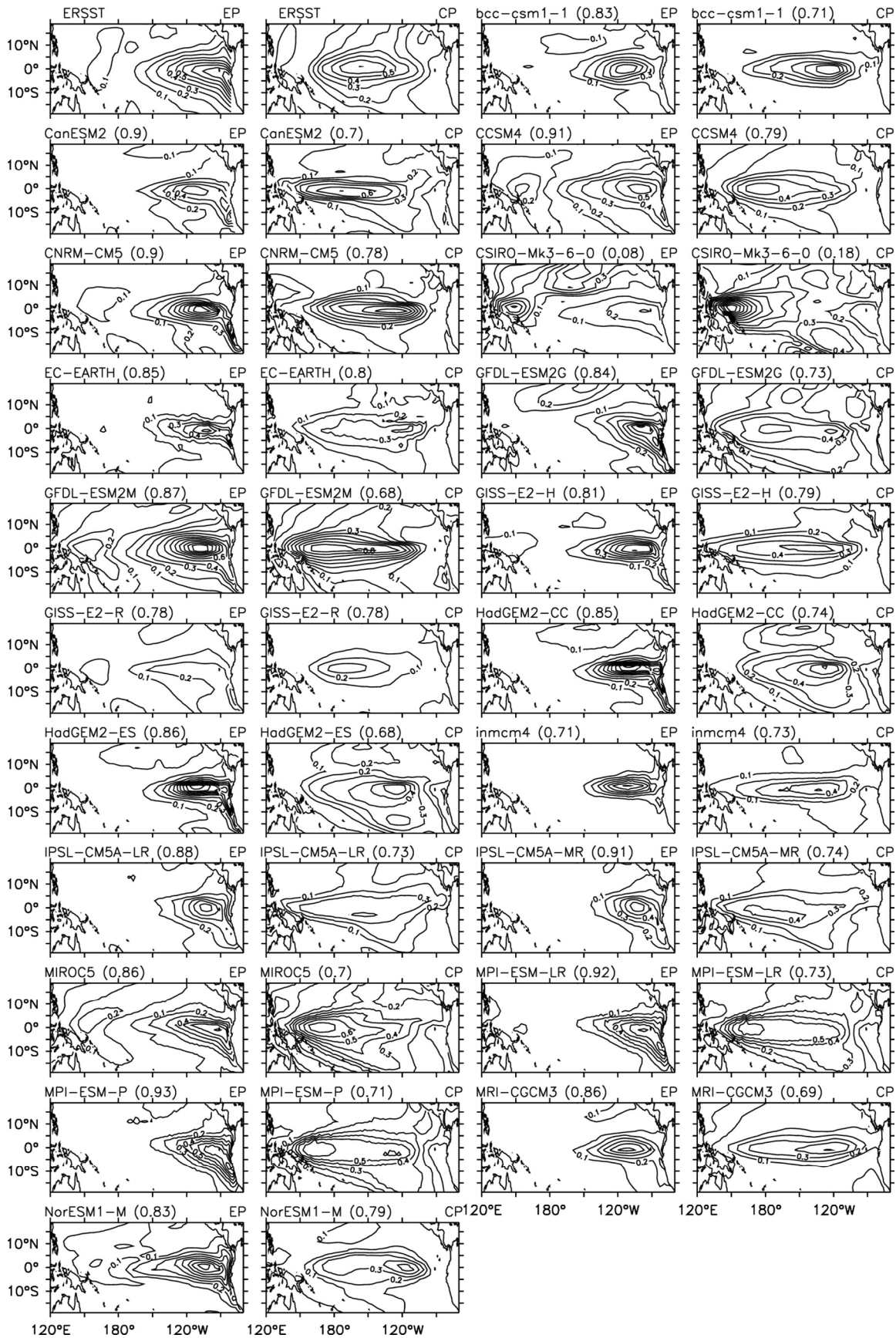
**Figure 1.** Spatial patterns of the standard deviations of the first EOF mode for the CP ENSO and EP ENSO calculated from observations and 20 CMIP5 models. The observations correspond to the ERSST dataset. Pattern correlations between models and observations are also shown in parentheses.
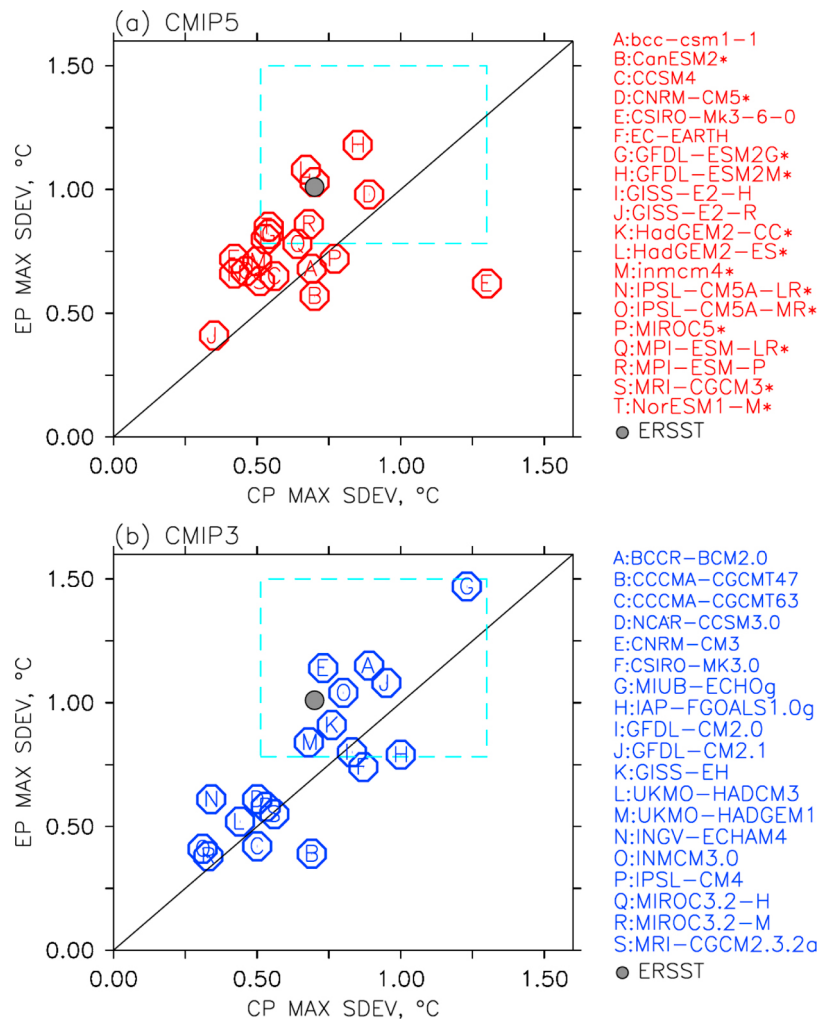
**Figure 2.** Scatter plots of maximum standard deviation from (a) CMIP5 and (b) CMIP3 models (reproduced from *Yu and Kim* [2010, Figure 2a]). The blue dashed lines indicate the lower limit of the 95% significance interval of the observed ENSO intensities based on an F-test. The names of the models used in the analyses are provided. The CMIP5 models that provide SST output from all the pre-industrial, historical, and RCP4.5 simulations are indicated by an asterisk.

difference for the CP ENSO, on the other hand, is less statistically significant (from 0.24 to 0.21). Figure 3 also indicates that the multi-model mean of both the EP and CP ENSO intensities are not very different between CMIP3 and CMIP5 models. In both generations of the CMIP models, the multi-model means of CP ENSO intensity are very close to the observed value (indicated by the dashed-line in the figure), but the multi-model means of the EP ENSO are only about half of the observed intensity. Therefore, though the CMIP5 models have smaller inter-model discrepancies in the simulation of the two types of ENSO, challenges remain in producing a realistically strong EP ENSO in these coupled climate models.

[9] We next examine the response of two types of ENSO to changes in atmospheric $CO_2$ concentrations using the thirteen CMIP5 models that provide SST outputs from the pre-industrial, historical, and RCP4.5 runs. Seven of them (CNRM-CM5, GFDL-ESM-2G, GFDL-ESM2M, HadGEM2-CC, HADGEM2-ES, MPI-ESM-LR, and Nor-ESM1-M) are among the nine CMIP5 models that produce strong EP and CP ENSOs. This group of seven models is used to produce

the "best model ensemble" for projecting the response of the two types of ENSO to the ongoing and possible future global warming. Figure 4a shows the "best model mean" of the EP and CP intensities and their ratio (CP/EP) in the pre-industrial, historical, and RCP4.5 simulations. The figure
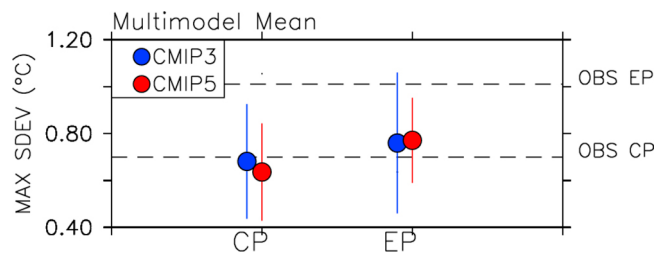


**Figure 3.** The multi-model ensemble mean of the intensities of the two types of ENSO from the CMIP3 models (blue) and the CMIP5 models (red). Inter-model deviations are indicated by vertical lines. The observed intensities are indicated by dashed lines.
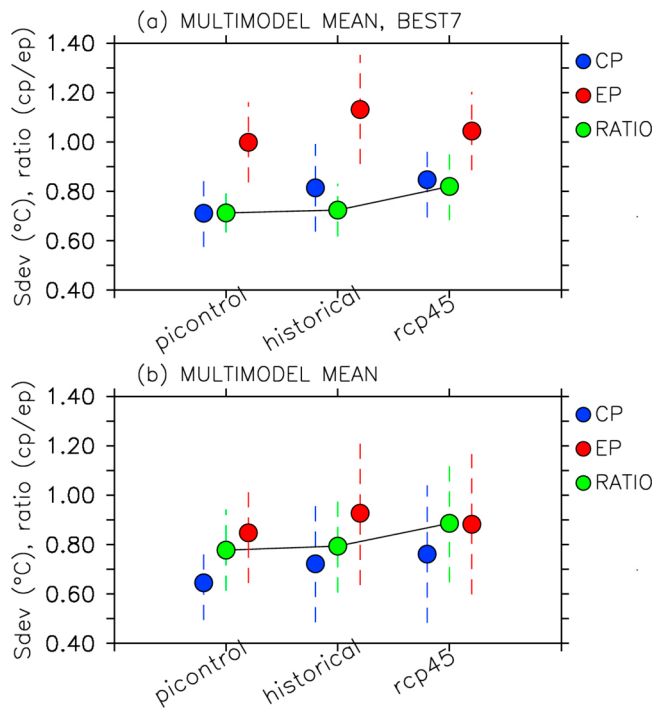
**Figure 4.** Multi-model mean of EP and CP intensities and the CP-to-EP ratio from the pre-industrial, historical, and RCP4.5 experiments for (a) the seven 'best' models, and (b) all thirteen models.

shows that the intensity of CP ENSO increases gradually from the pre-industrial simulation to the historical simulation and the RCP4.5 projection, while the intensity of EP ENSO increases from the pre-industrial simulation to the historical simulation but then decreases in the RCP4.5 projection. Since the best-model means of the EP and CP ENSO intensities show similar rates of increase from the pre-industrial to historical simulations, the CP-to-EP intensity ratio does not change much between these two runs. On the other hand, a sharp decrease in the EP ENSO intensity and a gradual increase in the CP ENSO intensity result in an increase in the ratio from the historical simulation to the RCP4.5 projection. As shown in Figure 4b, similar tendencies are also found when all the thirteen CMIP5 models are used to calculate the model ensemble means. It is interesting to note that in the RCP4.5 warming scenario, the intensity of the CP ENSO will increase to close to 80% (based on the best-model means) or 90% (based on the all-model means) of the EP ENSO intensity.

## 4. Summary and Discussion

[10] In this study we assessed the ability of the CMIP5 models in simulating the EP and CP types of ENSO. We find that close to 50% of the CMIP5 models still cannot simulate realistically strong EP and CP ENSOs, as was the case for the CMIP3 models. Furthermore, it is more difficult for the models to reproduce the observed EP ENSO intensity than the observed CP ENSO intensity. However, some encouraging improvements in the simulations of the two types of ENSO were found in the CMIP5 models. First of all, the simulated spatial patterns of both types of ENSO in the CMIP5 models are improved compared to the CMIP3 models according to

a pattern correlation coefficient analysis of the simulated and observed ENSO SST anomalies. Secondly, the inter-model differences in the intensities of the two types of ENSO are reduced among the CMIP5 models relative to the differences among the CMIP3 models. The decrease in the inter-model discrepancies (and hence the improvement in the consistency of model performance) is particularly significant for the simulations of the EP ENSO intensity. We also conclude that the responses of the two types of ENSO to increases in atmospheric $CO_2$ concentrations are different. The CP ENSO intensity is found to increase gradually from the pre-industrial simulation to the historical simulation and to the RCP4.5 projection, while the EP ENSO intensity is found to increase and then decrease during these three climate conditions. However, it should be cautioned that the changes of ENSO intensities from the pre-industrial, historical, to projected simulations are smaller than the standard deviation among the CMIP5 models.

[11] This study did not examine the cause(s) of the different responses of the two types of ENSO to global warming, which would require an extensive examination of both atmospheric and oceanic processes in the CMIP5 models. This issue is beyond the scope of this paper. It is possible that the different responses imply different generation mechanisms underlying the CP and EP ENSOs. Whereas the EP ENSO shares many characteristics with the canonical ENSO, whose underlying dynamics are known to rely on thermocline variations, the underlying dynamics of the CP ENSO have been suggested to potentially involve forcing from the extratropical atmosphere [*Kao and Yu*, 2009; *Yu et al.*, 2010; *Yu and Kim*, 2011; *Kim et al.*, 2012] and zonal ocean advection in the ocean mixed layer [*Kug et al.*, 2009; *Yu et al.*, 2010]. These dynamical processes may be affected differently by global warming and result in the different responses. Further analyses are needed to examine this hypothesis.

[13] The Editor thanks the two anonymous reviewers for assisting in the evaluation of this paper.

## References

Ashok, K., S. Behera, A. S. Rao, H. Weng, and T. Yamagata (2007), El Niño Modoki and its teleconnection, *J. Geophys. Res.*, *112*, C11007, doi:10.1029/2006JC003798.

Ding, Q., E. J. Steig, D. S. Battisti, and M. Küttel (2011), Winter warming in West Antarctica caused by central tropical Pacific warming, *Nat. Geosci.*, *4*, 398–403, doi:10.1038/ngeo1129.

Ham, Y.-G., and J.-S. Kug (2012), How well do current climate models simulate two types of El Niño?, *Clim. Dyn.*, doi:10.1007/s00382-001-1157-3, in press.

Kao, H.-Y., and J.-Y. Yu (2009), Contrasting eastern-Pacific and central-Pacific types of El Niño, *J. Clim.*, *22*, 615–632, doi:10.1175/2008JCLI2309.1.

Kim, H.-M., P. J. Webster, and J. A. Curry (2009), Impact of shifting patterns of Pacific Ocean warming on North Atlantic tropical cyclones, *Science*, *325*, 77–80, doi:10.1126/science.1174062.

Kim, S. T., J.-Y. Yu, A. Kumar, and H. Wang (2012), Examination of the two types of ENSO in the NCEP CFS model and its extratropical associations, *Mon. Weather Rev.*, doi:10.1175/MWR-D-11-00300.1, in press.

Kug, J.-S., F.-F. Jin, and S.-I. An (2009), Two types of El Niño events: Cold tongue El Niño and warm pool El Niño, *J. Clim.*, *22*, 1499–1515, doi:10.1175/2008JCLI2624.1.

Larkin, N. K., and D. E. Harrison (2005), On the definition of El Niño and associated seasonal average U.S. weather anomalies, *Geophys. Res. Lett.*, *32*, L13705, doi:10.1029/2005GL022738.

Lee, T., and M. J. McPhaden (2010), Increasing intensity of El Niño in the central-equatorial Pacific, *Geophys. Res. Lett.*, *37*, L14603, doi:10.1029/2010GL044007.

Lee, T., W. R. Hobbs, J. K. Willis, D. Halkides, I. Fukumori, E. M. Armstrong, A. K. Hayashi, W. T. Liu, W. Patzert, and O. Wang (2010), Record warming in the South Pacific and western Antarctica associated with the strong central-Pacific El Niño in 2009–10, *Geophys. Res. Lett.*, *37*, L19704, doi:10.1029/2010GL044865.

Meehl, G. A., et al. (2007), The WCRP CMIP3 multimodel dataset: A new era in climate change research, *Bull. Am. Meteorol. Soc.*, *88*, 1383–1394, doi:10.1175/BAMS-88-9-1383.

Mo, K. (2010), Interdecadal modulation of the impact of ENSO on precipitation and temperature over the United States, *J. Clim.*, *23*, 3639–3656, doi:10.1175/2010JCLI3553.1.

Smith, T. M., and R. W. Reynolds (2003), Extended reconstruction of global sea surface temperatures based on COADS data (1854–1997), *J. Clim.*, *16*, 1495–1510, doi:10.1175/1520-0442-16.10.1495.

Taylor, K. E., R. J. Stouffer, and G. A. Meehl (2012), An overview of CMIP5 and the experimental design, *Bull. Am. Meteorol. Soc.*, *93*, 485–498, doi:10.1175/BAMS-D-11-00094.1.

Trenberth, K., and D. P. Stepaniak (2001), Indices of El Niño evolution, *J. Clim.*, *14*, 1697–1701, doi:10.1175/1520-0442(2001)014<1697:LIOENO>2.0.CO;2.

Wang, C., and R. H. Weisberg (2000), The 1997–98 El Niño evolution relative to previous El Niño events, *J. Clim.*, *13*, 488–501, doi:10.1175/1520-0442(2000)013<0488:TENOER>2.0.CO;2.

Yu, J.-Y., and H.-Y. Kao (2007), Decadal changes of ENSO persistence barrier in SST and ocean heat content indices: 1958–2001, *J. Geophys. Res.*, *112*, D13106, doi:10.1029/2006JD007654.

Yu, J.-Y., and S. T. Kim (2010), Identification of central-Pacific and eastern-Pacific types of El Niño in CMIP3 models, *Geophys. Res. Lett.*, *37*, L15705, doi:10.1029/2010GL044082.

Yu, J.-Y., and S. T. Kim (2011), Relationships between extratropical sea level pressure variations and central-Pacific and eastern-Pacific types of ENSO, *J. Clim.*, *24*, 708–720, doi:10.1175/2010JCLI3688.1.

Yu, J.-Y., H.-Y. Kao, and T. Lee (2010), Subtropics-related interannual sea surface temperature variability in the equatorial central Pacific, *J. Clim.*, *23*, 2869–2884, doi:10.1175/2010JCLI3171.1.